IEEE Access
Multidisciplinary | Rapid Review | Open Access Journal

Received November 14, 2017, accepted December 11, 2017, date of publication December 29, 2017,
date of current version February 14, 2018.

Digital Object Identifier 10.1109/ACCESS.2017.2786271

Drusen Segmentation From Retinal Images via Supervised Feature Learning

XIUXIU REN[1], YUANJIE ZHENG[1,2,3,4,5], YANNA ZHAO[1], CHAO LUO[1], HONG WANG[1], JIAN LIAN[1,6], AND YUNLONG HE[1]

[1]School of Information Science and Engineering, Shandong Normal University, Jinan 250358, China
[2]Key Laboratory of Intelligent Computing and Information Security in Universities of Shandong, Shandong Normal University, Jinan 250358, China
[3]Institute of Biomedical Sciences, Shandong Normal University, Jinan 250358, China
[4]Shandong Provincial Key Laboratory for Distributed Computer Software Novel Technology, Shandong Normal University, Jinan 250358, China
[5]Key Laboratory of Intelligent Information Processing, Shandong Normal University, Jinan 250358, China
[6]Department of Electronic Engineering Information Technology, Shandong University of Science and Technology, Jinan 250031, China

Corresponding author: Yuanjie Zheng (zhengyuanjie@gmail.com)

This work was supported in part by the Natural Science Foundation of China under Grant 61572300, in part by the Natural Science Foundation of Shandong Province in China under Grant ZR2014FM001 and Grant ZR2016FQ06, in part by the Taishan Scholar Program of Shandong Province in China under Grant TSHW201502038, and in part by the China Postdoctoral Science Foundation under Grant 2017M612335.

ABSTRACT This paper presents a supervised feature learning method to learn discriminative and compact descriptors for drusen segmentation from retinal images. This method combines generalized low rank approximation of matrices with supervised manifold regularization to learn new features from image patches sampled from retinal images. The learned features are closely related to drusen and potentially free from information that is redundant in distinguishing drusen from background. The learned feature representations are then vectorized and used to train a support vector machine (SVM) classifier. Finally, the obtained SVM classifier is employed to classify the pixels in the test images as drusen or non-drusen. The performance of the proposed method is validated on the STARE and DRIVE databases, where it achieves an average sensitivity/specificity/accuracy of 90.03%/97.06%/96.92% and of 87.41%/94.93%/94.81%, respectively. We also experimentally compare the proposed method with the several representative state-of-the-art drusen segmentation techniques and find that it generates superior accuracy.

INDEX TERMS Age-related macular degeneration, drusen segmentation, feature learning, retinal images.

I. INTRODUCTION

Age-related macular degeneration (AMD) is a degenerative eye disease and is the most common cause of legal blindness for people over 50 in developed countries [1]–[3]. Drusen are yellow-white spots located beneath the layer of retinal pigment epithelium (RPE) cells. Drusen are considered to be a specific physical sign of early AMD [4], [5] because they play a major role in the progression of advanced AMD [3], [6], [7]. Many longitudinal studies have discovered that drusen in a larger size or number may result in a degeneration of RPE cells followed by a decline in central visual acuity [8]–[10]. Moreover, the total drusen area is positively correlated with the risk of progression to advanced AMD [11]. Therefore, the clinical assessment of drusen characteristics is helpful for determining whether and when a patient will suffer visual loss or blindness from AMD.

Drusen segmentation aims to find the location and area of drusen on fundus images. It is a highly challenging task in retinal fundus image analysis. The associated challenges can be attributed to three reasons. First, color variations over color fundus images, which are caused by choroidal pigmentation, can confuse the observer in distinguishing drusen from the optic disc or background. Second, drusen might vary significantly in shape and size, making the detection and segmentation quite difficult. Third, nonuniform illumination or other image artifacts may cause unpredictable variations in image intensity or color.

To address the difficulties associated with drusen segmentation, researchers have proposed a large variety of approaches over the past twenty years. The methods for drusen segmentation can primarily be classified into three categories. The first category is based on the frequency domain by taking advantage of Fourier transform [12], amplitude-modulation frequency modulation or wavelet [13]. The second category focuses on thresholding techniques, e.g., local thresholds [14], [15], global thresholds [16] and fuzzy logic

2169-3536 © 2017 IEEE. Translations and content mining are permitted for academic research only.
Personal use is also permitted, but republication/redistribution requires IEEE permission.
See http://www.ieee.org/publications_standards/publications/rights/index.html for more information.

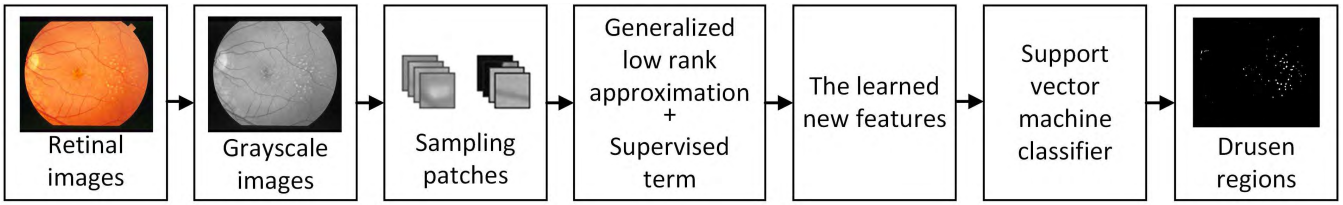

FIGURE 1. The flowchart of our proposed drusen segmentation method.

thresholds [17]. The third category extracts features from an image and distinguishes drusen from other tissues based on these features. For the third type of methods, a crucial factor in achieving a successful segmentation lies in the discriminative ability of the feature(s) being used [18]–[21]. The features currently adopted in these methods include intensity differences [22], biologically inspired feature (BIF) [23], eigen vector [24], [25], and so forth. However, these hand-crafted features are not always discriminative enough to accurately detect drusen due to the aforementioned challenges.

Many cases have shown that the classification performance can be significantly improved by applying discriminant learning techniques [26]–[30] compared with using hand-crafted features. For example, Wang *et al.* [28] obtained supervised kernel descriptors (SKDES) by embedding the image label information into the design of the patch-level kernel, and the performance on image classification benchmarks was improved. Lei *et al.* [27] learned a discriminant face descriptor (DFD) in a data-driven way, which incorporates the discriminate image filter and the optimal soft sampling learning for face recognition. Simonyan *et al.* [26] proposed a framework to obtain a new descriptor by learning a sparse pooling region configuration and a low-rank projection for the selected pooling regions. Zhen *et al.* [31] presented a novel supervised descriptor learning algorithm for multi-output regression, which is formulated as generalized low rank approximations of matrices with a supervised manifold regularization. The power of discriminant learning lies in its ability to extract discriminative features while removing irrelevant and redundant information by transforming raw features into a new low-dimensional space aligned with the targets. Disregarding the progression of feature learning in image classification, we find that it has rarely been used in drusen segmentation.

In this paper, we present a supervised feature learning (SFL) framework for drusen segmentation, which is achieved by adjusting the multi-output regression model for image classification in [31] to the problem of image segmentation. Compared with hand-crafted features, the features learned via the proposed framework are capable of extracting properties related to drusen while removing other redundant information, being more discriminative and compact. The proposed framework consists of three main steps. In the first step, patches are sampled from the grayscale retinal images and treated as the training data. In the second step, the SFL algorithm combines the benefits of generalized low rank approximations of matrices (GLRAM) and supervised manifold regularization (SMR) to learn a new descriptor. The learned descriptors are vectorized and fed into a support vector machine (SVM) to train a classifier. Finally, the obtained SVM classifier is employed to classify the pixels in the test image as drusen or non-drusen. The experimental results show that our method outperforms state-of-the-art methods.

II. METHOD

Based on the raw image pixel intensities of the training data and by following the supervised descriptor learning strategy of [31], the proposed SFL algorithm is applied to generate discriminative and compact feature representations for accurate and efficient drusen segmentation. The SFL algorithm is formulated as GLRAM and SMR. The GLRAM is to learn a low-dimensional representation by reducing the dimension of a sequence of matrices, while the SMR takes full advantage of the supervision to improve the discrimination of feature representation. The flowchart of the proposed method is shown in Fig. 1.

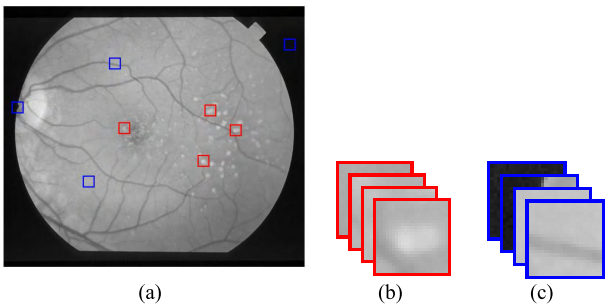

FIGURE 2. Training data. (a): A whole training image, where red windows are training drusen patches and blue windows are training background patches. (b): Drusen patches. (c): Background patches.

A. PROBLEM STATEMENT

Given color training images, we first convert them into grayscale images by eliminating the hue and saturation information while retaining the luminance. Based on the grayscale training images and the corresponding ground truth, n patches are randomly sampled from drusen and background regions. Examples of the training patches are shown in Fig. 2. The training patches and the corresponding labels are defined as

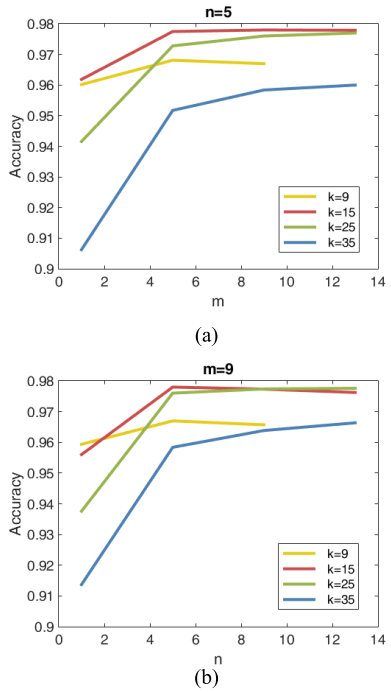

FIGURE 3. Performance with different patch sizes and dimensions. k is the patch size, m is the reduced dimensionality by U, n is the reduced dimensionality by V.

$\{S_1, S_2, \cdots, S_n\}$ and $Ł_i \in (0, 1)$, $1 \leq i \leq n$, where n is the number of training patches. Each S_i has a size of $k \times k$. The patch label L_i is 1 if the center pixel is drusen; otherwise, the label is 0. Each patch is represented in its native matrix representation rather than vectors as inputs, which can be any form of matrix representation. We propose using the raw image pixel intensities for simplicity. We aim to compute a new discriminative and low-dimensional representation of each $S_i \in R^{r\times c}$ by adding a supervised term. The obtained low rank approximations of matrices are vectorized as the final descriptor and fed into the SVM classifier.

B. GENERALIZED LOW-RANK APPROXIMATION

Low-rank approximations of matrices have become an important tool for extracting correlations and removing noise from data. To obtain low-dimensional representations of training patches, GLRAM [31], [32] is used to reduce the dimensions of matrices. Compared with other traditional low-rank approximation methods [33]–[35], the GLRAM plays a role in the matrix representation of images directly rather than using a vector representation. A generalized low-rank approximation problem is to approximate a sequence of matrices with low rank, as shown by the following minimization problem:

$$\begin{aligned} &\arg\min_{U,V,\{A\}_{i=1}^{n}} \frac{1}{n}\sum_{i=1}^{n} \|S_i - UA_iV^T\|_F^2 \\ &s.t.\ U^TU = I_{l_1} V^TV = I_{l_2} \end{aligned} \tag{1}$$

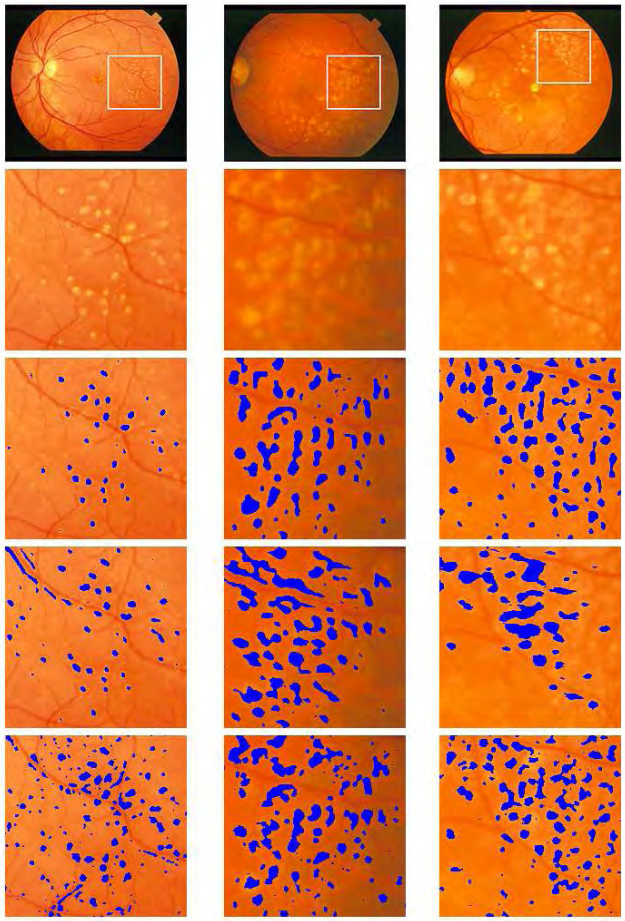

FIGURE 4. Segmentation results of different types of drusen on the STARE database. From top to bottom: the entire original fundus image, drusen region in the retinal color image, segmentation results of our method, segmentation results of Liu et al., and segmentation results of HALT.

The goal of Eq. 1 is to find two matrix transformations $U \in R^{r\times l_1}$ and $V \in R^{c\times l_2}$ that approximate each $S_i \in R^{r\times c}$ to a matrix $A_i \in R^{l_1\times l_2}$, for $1 \leq i \leq n$, such that $A_i = US_iV^T$ is an approximation of S_i. In Eq. 1, $\|\|_F$ is the Frobenius norm, which is a natural similarity metric between matrices. U and V are considered as linear transformations of matrix form. I_{l_1} and I_{l_2} denote identity matrices, whose sizes are $l_1 \times l_1$ and $l_2 \times l_2$, respectively, and the constraints $U^TU = I_{l_1}$ and $V^TV = I_{l_2}$ are added to Eq. 1 for avoiding redundancy in the approximations.

Eq. 1 aims to find the optimal transformations U and V such that the original high-dimensional space is preserved in the low-dimensional space $\{A\}_{i=1}^{n}$. Although $\{A\}_{i=1}^{n}$ have low dimension, they do not have sufficient discriminative ability. To obtain more discriminative representations of $\{A\}_{i=1}^{n}$, we incorporate the patch labels to achieve a more discriminative representation as follows.

C. SUPERVISED TERM

We first construct a weighted graph G with n nodes, one for each patch, and the set of edges connecting neighboring nodes

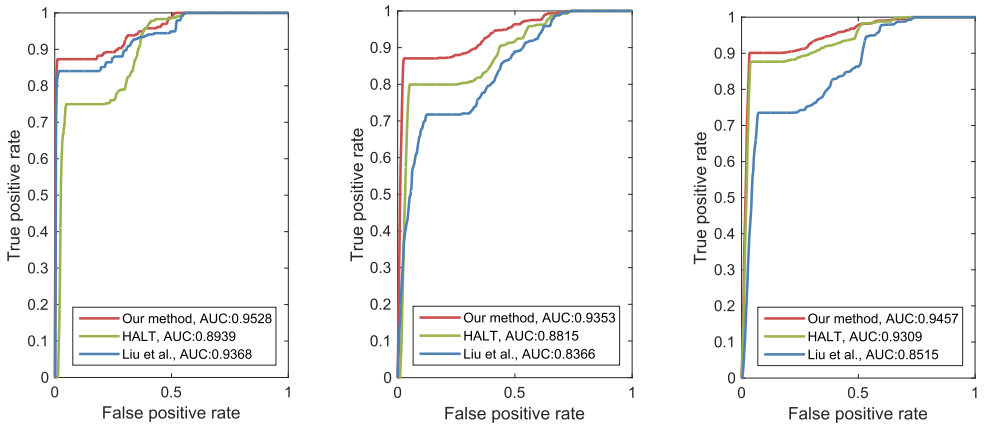

FIGURE 5. ROC curves of our method, HALT [14] and Liu et al.'s method [4] in drusen classification on three representative images.

using the method in [36]. Specifically, an edge between nodes i and j is constructed if i is among the k nearest neighbors of j or j is among the k nearest neighbors of i. M denotes the similarity matrix, which is a sparse symmetric $n \times n$ matrix of nonnegative elements with M_{ij} having the weight of the edge joining vertices i and j. If nodes i and j are connected, then M_{ij} is computed by using a heat kernel:

$$M_{ij} = e^{\frac{-\|L_i - L_j\|^2}{\alpha}} \quad i, j = 1, 2, \cdots, n \tag{2}$$

where α is a parameter and L is the label of the corresponding training patches. We minimize the following term in low-rank space:

$$\sum_{i,j} \|A_i - A_j\|_F^2 M_{ij} \tag{3}$$

where $\{A\}_{i=1}^n$ characterizes the low-rank approximation and preserves the intrinsic local geometrical structure of the target space. M measures the similarities between two training patches and reflects the manifold structure of the target space. Minimizing Eq. 3 can inject the discrimination into the low-rank representation via the supervised labels. By adding the supervised term, training patches with the same labels tend to be classified into one part, whereas those with different labels tend to be another part. This increases the discriminative ability of the learned feature representation.

D. LEARNING NEW FEATURE REPRESENTATION

In summary, our model is obtained by combining GLRAM with the SMR term in Eq. 1 and Eq. 2:

$$\begin{aligned} &\arg\min_{U,V,\{A\}_{i=1}^n} \frac{1}{n}\sum_{i=1}^{n} \|S_i - UA_iV^T\|_F^2 + \gamma \sum_{i,j} \|A_i - A_j\|_F^2 M_{ij} \\ &s.t.\ U^TU = I_{l_1} V^TV = I_{l_2} \end{aligned} \tag{4}$$

where $\gamma \in (0, \infty)$ is used to control the trade-off between the approximation accuracy and the discriminative ability. The GLRAM term aims to reduce the dimension to find a low-rank approximation of the input patch matrices $\{S\}_{i=1}^n$, while the second term introduces supervision to improve the discrimination of the low-rank approximation $\{A\}_{i=1}^n$. The objective of SFL is to extract discriminative features that are robust to drusen variations.

Due to the difficulty of directly solving the above function, an iterative algorithm via an alternate optimization [31] is used to obtain the optimal solution of U, V and $\{A\}_{i=1}^n$. Considering that the truncated singular value decomposition (SVD) can obtain the best approximation of given matrices concerning the Frobenius norm [32], [34], SVD is adopted in our algorithm to solve the standard eigen decomposition. The details of the iterative algorithm are presented in APPENDIX.

E. APPLICATION OF DRUSEN SEGMENTATION

Based on the computed U and V, the overall classification scheme includes a training procedure and a testing procedure. To leverage the strength of SVM for the classification task, LibSVM with radial basis function (RBF) kernel is employed in our experiments.

- The training procedure: With the learned transformations U and V, the patches are projected onto $l_1 \times l_2$ approximation matrices $\{A\}_{i=1}^n$. These matrices are then transformed into vectors of $l_1 \times l_2$ dimension, which are considered as feature vectors to train a classifier. Based on the feature vectors and corresponding labels above, an SVM classifier is obtained.
- The testing procedure: Given a test image I from the evaluation dataset, we represent each pixel by a $k \times k$ patch with the raw image pixel intensities. Using U and V, we obtain the low-rank approximation $\{A\}_{i=1}^n$ of all the patches. The final descriptor of each pixel is obtained by vectorizing $\{A\}_{i=1}^n$ and fed into the SVM classifier. The pixel is labeled 1 if its feature vector is classified as drusen; otherwise, the pixel is labeled 0.

III. EXPERIMENTS AND RESULTS

A. DATA

The proposed SFL is evaluated on the publicly available STARE database [37]. This database was used to validate various retinal image processing algorithms, including

TABLE 1. The compared results based on statistical analysis.

	Our method			HALT			Liu et al.		
Image	%Se	%Spe	%Acc	%Se	%Spe	%Acc	%Se	%Spe	%Acc
im1	87.30	98.01	97.91	86.42	95.89	95.77	84.04	94.17	94.15
im2	89.85	93.20	93.12	79.55	93.59	93.27	86.98	92.56	92.53
im3	86.05	95.27	94.95	79.83	91.47	91.16	88.82	77.55	77.94
im4	93.98	95.48	95.38	90.10	90.63	90.61	78.02	93.20	93.17
im5	93.91	93.69	93.67	78.92	90.84	90.71	76.26	79.00	78.98
im6	92.80	94.61	94.58	93.27	92.54	92.55	87.19	87.13	87.12
im7	89.08	96.67	96.54	90.88	91.40	91.37	77.49	84.51	84.48
im8	87.06	97.09	96.95	84.37	94.18	94.04	81.18	95.08	94.88
im9	89.72	98.37	98.32	87.72	89.44	89.43	86.48	96.15	96.09
im10	87.44	97.46	97.39	84.14	91.75	91.70	78.81	92.86	92.77
im11	90.11	95.01	94.93	87.67	94.56	94.45	83.89	89.64	89.54
im12	90.34	97.74	97.56	88.76	92.49	92.39	77.59	90.60	90.27
im13	91.49	98.56	98.48	86.51	91.30	91.27	82.56	98.41	98.30
im14	93.74	97.35	97.29	87.35	98.89	98.70	81.96	93.69	93.49
im15	93.65	97.95	97.94	88.56	95.19	95.16	95.97	96.12	96.09
im16	88.68	97.92	97.84	86.48	92.54	92.49	77.56	96.91	96.75
im17	90.24	97.31	96.94	85.66	88.04	87.91	89.61	93.32	93.13
im18	92.86	98.13	98.11	88.38	95.24	95.19	91.22	96.38	96.56
im19	91.10	94.39	94.37	79.98	94.19	94.12	84.15	97.42	97.36
im20	89.60	94.87	94.74	82.24	88.98	88.82	84.20	91.61	91.43
im21	91.03	96.58	96.49	83.98	93.27	93.12	90.88	90.49	90.50
im22	87.07	98.61	98.47	85.83	98.69	98.54	88.14	95.13	95.05
im23	92.11	97.41	97.31	93.64	93.18	93.11	89.05	95.90	95.87
im24	95.21	96.40	96.37	85.19	87.82	87.76	84.29	90.39	90.33
im25	88.84	98.60	97.91	77.84	90.31	89.43	81.36	89.65	89.61
im26	91.50	99.64	99.32	86.02	91.22	91.02	91.39	97.86	97.79
im27	82.18	94.78	94.53	88.72	92.42	92.34	86.15	93.53	93.47
im28	78.14	99.36	99.34	80.30	95.34	95.32	82.24	88.92	88.90
im29	93.90	91.93	91.96	78.91	94.35	94.10	98.20	73.26	73.65
im30	97.92	93.43	93.45	86.42	95.89	95.87	87.18	96.72	96.68
im31	86.64	96.51	96.36	82.67	95.87	95.83	87.67	97.93	97.91
im32	89.40	98.93	98.83	88.42	90.99	90.96	86.93	94.31	94.28
im33	86.17	99.58	99.37	82.01	99.45	99.18	77.34	99.63	99.28
im34	93.96	98.46	98.39	92.53	95.64	95.59	73.41	94.38	93.86
im35	93.02	99.28	99.27	82.37	96.22	96.20	76.60	97.44	97.36
im36	91.69	98.92	98.71	83.92	97.70	97.53	82.54	99.05	98.85
im37	85.05	99.82	99.55	72.83	79.19	79.08	75.76	92.15	91.79
im38	92.85	97.09	96.90	88.14	91.16	91.02	89.75	87.32	87.58
im39	83.63	98.44	97.82	80.47	96.79	96.11	88.24	97.05	96.99
im40	89.55	99.31	99.19	92.90	98.41	98.37	82.06	98.23	98.17
im41	92.27	97.14	97.01	90.63	87.37	87.58	82.62	93.74	93.61
Average	90.03	97.06	96.92	85.37	93.03	92.91	84.28	92.66	92.59

vessel segmentation [38], optic disc localization [39], generic lesion detection [40], and so forth. The STARE images were collected using a TopCon TRV-50 fundus camera with an FOV of 35 degrees. These fundus images do not have spatial resolution information because the interior of the eye being imaged is semi-spherical [41]. It includes 400 retinal fundus images, and the size of each image is 700 $\times$ 605 pixels. Sixty-three images are clinically verified as containing drusen. From the images containing drusen, 46 are randomly selected to test our approach. In detail, 5 representative images are treated as training data, and the remaining 41 images are the testing data.

The public database of DRIVE [42], [43] is also used to validate our methodology. This database contains a total of 40 RGB color retinal images. These retinal images are captured by a Canon CR5 non-mydriatic 3-CCD camera (Canon, Tokyo, Japan) with a 45 degree field of view (FOV). The size of each image is 768$\times$584 pixels. In the following experiments, 9 retinal images are tested on this database. Drusen are manually marked on test images with the help of the drawing tool in the computer software. These marks are treated as the ground truth, and their locations are compared with the ones obtained by SFL and the comparison methods.

B. EXPERIMENTAL SETTING

In our experiments, the parameter γ is set to be 1 for a trade-off between the reconstruction accuracy and discriminative ability. In fact, the iterative solution converges fast within few iterations. Specifically, we choose 6 iterations to achieve a satisfactory result in our experiments. In addition, the patch size and reduced dimensionality have a clear influence on the final segmentation results, and we will compare them in section D.

C. EVALUATION

To quantitatively measure the performance of the proposed method, the results of drusen segmentation are measured by the commonly used sensitivity (Se), specificity (Spe), and accuracy (Acc) [44]–[46]. Se is used to measure the rate of true positive detection, Spe measures the rate of false positive detection, and Acc indicates the ratio of the total correctly identified pixels. To be more intuitive, we plot the receiver operating characteristics (ROC) and compute the area under the curve (AUC) values.

D. RESULTS

We first test our algorithm by fully utilizing the GLRAM and SMR. We change the patch size k and find that it has a clear impact on the performance. Comparing the performance when $k = 9$, 15, 25, and 35 under various reduced dimensionalities, we can observe different classification accuracies, as shown in Fig. 3. As shown, our method performs best when $k = 15$ (red lines), and we fix k to 15 in the following experiments.

The reduced dimensionality also affects the performance. Since the reduced dimensionality depends on both parameters m and n, we conduct experiments to test the influence of one parameter by keeping the other parameter fixed. Figs. 3 (a) and (b) indicate that our method achieves the best performance when $m = 9$ and $n = 5$, and these parameters are kept fixed in all the experiments.

On the STARE dataset, we compare the performance of our algorithm with two drusen segmentation methods. The first one is the state-of-the-art method HALT [14]. This method employs a multilevel histogram equalization scheme and develops an adaptive local histogram to identify an appropriate local threshold (HALT) to segment each drusen. The second one is the method proposed by Liu *et al.* [4]. This method extracts some features at local maximum points and trains a classifier from the weakly labeled data to classify each maximum point as drusen or non-drusen. We compare the segmentation results and Se, Spe, Acc, and AUC.

Fig. 4 shows the segmentation results on three representative images from the STARE dataset: one image with small sparse drusen, the second one with large drusen, and the third one with vague small and large drusen. The segmentation results are satisfactory in all cases in that the background areas are segmented and the drusen are correctly isolated. In general, the presence of vessels and their interaction in intensity with drusen increases the difficulties of segmentation. Our algorithm overcomes this problem due to the learned discriminative and compact features from fundus images that can separate drusen from vessel distributions. To be more intuitive, we plot the ROC curves and compute the AUC of these segmentation techniques in Fig. 5. It is clear that our algorithm is superior to the comparison algorithms.

TABLE 2. Comparison results of the proposed method and some existing methods.

Methods	Dataset	No. of images	%Se	%Spe	%Acc
Our method	STARE	41	90.03	97.06	96.92
	DRIVE	9	87.41	94.93	94.81
[48]	ACHIKO-D350	64	68	94	-
[49]	-	22	68	96	-
[50]	STARE and ARIA	36	82	91.3	93.2
[51]	-	12	74.94	81.17	79.59
[26]	-	30	84	76	82

To further demonstrate the effectiveness of the proposed method, the Se, Spe and Acc of SFL and the above two methods on the remaining 41 images are given. As previously mentioned, these images are selected randomly from the STARE dataset. All images reflect actual cases without any prior information on the status and extent of drusen. In Tab. 1, the three average indicators of SFL exceed 90%, 97% and 96%, which outperform those of the compared algorithms. As shown in Tab. 1, the proposed method outperforms the state-of-the-art techniques.

Our algorithm also performs well on the DRIVE dataset, as shown by the classification results on three representative retinal images in Fig. 6. In fact, we test 9 retinal images on the DRIVE dataset and achieve an average Se of 87.41%, an average Spe of 94.93% and an average Acc of 94.81%.

The comparative performance analysis of the proposed method with some existing methods is shown in Tab. 2. Note that not all the drusen detection methods have used the same datasets in Tab. 2. Liu *et al.* [47] used GrowCut to segment drusen based on local extreme points and related features. Mora *et al.* [48] detected drusen using a gradient-based segmentation algorithm and then fit modified Gaussian functions to evaluate the affected area. The method of Kumari and Mittal [49] combined mathematical morphology and Otsu's algorithm to detect drusen. Zheng *et al.* [25] proposed a set of new features and presented a learning-based detection scheme. In the method of Bhuiyan *et al.* [50], local intensity distribution, adaptive intensity thresholding and edge information were used to detect potential drusen areas. The experimental comparisons demonstrate the effectiveness of our method for drusen segmentation. These results can be attributed to the following aspects. First, the proposed supervised algorithm can effectively extract the most discriminative features related to drusen while removing the redundant information by the iterative algorithm. Second, the features learned with supervision by the iterative algorithm surpass the

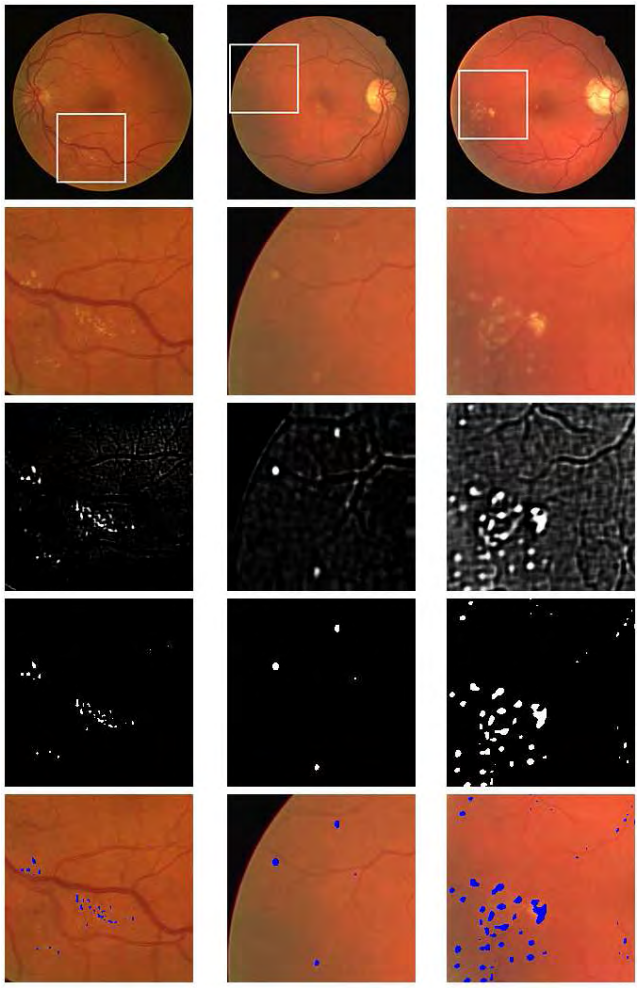

FIGURE 6. Segmentation results of three representative retinal images on the DRIVE database. From top to bottom: the entire original fundus image, drusen region in the retinal color image, posterior probability map after classification step, pixel clusters that are probable drusen, and objects that the algorithm classified as drusen overlaid on the original image.

hand-crafted features, particularly for drusen classification in fundus images. The satisfactory results demonstrate the great advantages of our method for drusen segmentation.

IV. CONCLUSION

In this paper, we propose a novel SFL algorithm for drusen segmentation from fundus images. The proposed algorithm can learn new features by leveraging the strengths of GLRAM and SMR, which reduces the dimension of image patches while improving the discriminative power. The learned features are distinguished from most handcrafted features in the sense that they are more compact and discriminative. An SVM classifier is trained by using these features, and then it classifies drusen pixels in new test images. Our algorithm is compared with state-of-the-art techniques, and the experimental results on a set of images with different classes and shapes of drusen demonstrate the effectiveness of our method in drusen segmentation.

APPENDIX
DETAILS OF THE ITERATIVE ALGORITHM

Due to the difficulty of directly solving the above function, an alternative objective function is found to obtain the optimal solution of U, V and $\{A\}_{i=1}^{n}$. Therefore, the first term in Eq. 4 is rewritten and simplified as follows according to [32]:

$$\begin{aligned}
&\frac{1}{n}\sum_{i=1}^{n}\|S_i - UA_iV^T\|_F^2 \\
&= \frac{1}{n}\sum_{i=1}^{n} trace((S_i - UA_iV^T)(S_i - UA_iV^T)^T) \\
&= \frac{1}{n}(\sum_{i=1}^{n} trace(S_iS_i^T) + \sum_{i=1}^{n} trace(A_iA_i^T) \\
&\quad - 2\sum_{i=1}^{n} trace(UA_iV^TS_i^T))
\end{aligned} \tag{5}$$

where the first term $\sum_{i=1}^{n} trace(S_iS_i^T) = \sum_{i=1}^{n}\|S_i\|_F^2$ is a constant because the $\{S\}_{i=1}^{n}$ is given above. Consequently, the minimization of Eq. 5 is equivalent to minimizing the following:

$$\frac{1}{n}(\sum_{i=1}^{n} trace(A_iA_i^T) - 2\sum_{i=1}^{n} trace(UA_iV^TS_i^T)) \tag{6}$$

It is easy to obtain that only if $A_i = U^TS_iV$, for $i = 1, \cdots, n$, does the function in Eq. 6 achieve the minimum. Hence, by substituting $A_i = U^TS_iV$ into Eq. 5 and removing the constant $\sum_{i=1}^{n} trace(S_iS_i^T)$, the minimization problem in Eq. 5 is equivalent to the following optimization problem:

$$\begin{aligned}
&\arg\max_{U,V} \frac{1}{n}\sum_{i=1}^{n}\|U^TS_iV\|_F^2 \\
&s.t.\ U^TU = I_{l_1} V^TV = I_{l_2}
\end{aligned} \tag{7}$$

Additionally, $A_i = U^TS_iV$ is added to the second term in Eq. 4, and a new alternative second term is obtained as follows:

$$\sum_{i,j}\|U^T(Si - Sj)V\|_F^2 M_{ij} \tag{8}$$

Combining Eq. 7 and Eq. 8, the final optimization function is obtained as follows:

$$\begin{aligned}
&\arg\max_{U,V} \frac{1}{n}\sum_{i=1}^{n}\|U^TS_iV\|_F^2 - \gamma\sum_{i,j}\|U^T(S_i - S_j)V\|_F^2 M_{ij} \\
&s.t.\ U^TU = I_{l_1}, \quad V^TV = I_{l_2}
\end{aligned} \tag{9}$$

For seeking the optimal solution of U and V, an iterative algorithm is provided to solve the objective function. Thus, objective function Eq. 9 is rewritten as follows:

$$\begin{aligned}
&\arg\max_{U,V} \frac{1}{n} trace(\sum_{i=1}^{n} U^TS_iVV^TS_i^TU) \\
&\qquad - \gamma\, trace(\sum_{i,j} U^T(S_i - S_j)VM_{ij}V^T(S_i - S_j)U) \\
&s.t.\ U^TU = I_{l_1}, V^TV = I_{l_2}
\end{aligned} \tag{10}$$

In fact, the above objective function naturally avoids the rank-deficit problem in the trace ratio form [51]. The GLRAM term ensures the reconstruction precision, and the SMR term improves the discrimination of the learned descriptor. Consequently, the SFL learns a new feature representation that has low dimension but high discrimination.

According to the above objective function, for a given V, an optimal U is calculated by using an iterative method. The maximum of Eq. 10 is equal to finding the maximum of $trace(U^T X_U U)$, where

$$X_U = \frac{1}{n}\sum_{i=1}^{n} S_i V V^T S_i^T - \gamma \sum_{i,j} (S_i - S_j) V M_{ij} V^T (S_i - S_j)^T \tag{11}$$

only if $U \in R^{r \times l_1}$ consists of l_1 eigenvectors of the matrix X_U corresponding to the largest l_1 eigenvalues. Additionally, the maximum can be considered as a special case of the more general optimization problem [52]. Similarly, for a given U, finding an optimal V is to solve the maximum of $trace(V^T X_V V)$, s.t. $V^T V = I_{l_2}$, where

$$X_V = \frac{1}{n}\sum_{i=1}^{n} S_i U U^T S_i^T - \gamma \sum_{i,j} (S_i - S_j)^T U M_{ij} U^T (S_i - S_j) \tag{12}$$

only if V consists of l_2 eigenvectors of the matrix X_V corresponding to the largest l_2 eigenvalues.

In detail, if an initial U is provided, the V is computed by finding the eigenvectors of the matrix X_V. With the computed V, the U is then updated by computing the eigenvectors of the matrix X_U. The procedure can be repeated until convergence, and the optimal U and V are finally obtained with the iterative procedure. Meanwhile, we obtain the A_i using the left and right transformation matrices U and V by $A_i = U^T S_i V$. The initial U_0 is important for the final solution. Experiments are performed, and it is found that $U_0 = (I_0, 0)^T$, where I_0 is the identity matrix, produces satisfactory results. Then, the obtained U_0 is used in our following experiments.

REFERENCES

[1] R. D. Jager, W. F. Mieler, and J. W. Miller, "Age-related macular degeneration," *New England J. Med.*, vol. 358, no. 24, pp. 2606–2617, 2008.

[2] S. Schmitz-Valckenberg, J. S. Steinberg, M. Fleckenstein, S. Visvalingam, C. K. Brinkmann, and F. G. Holz, "Combined confocal scanning laser ophthalmoscopy and spectral-domain optical coherence tomography imaging of reticular drusen associated with age-related macular degeneration," *Ophthalmology*, vol. 117, no. 6, pp. 1169–1176, 2010.

[3] F. G. Schlanitz *et al.*, "Performance of drusen detection by spectral-domain optical coherence tomography," *Invest. Ophthalmol. Vis. Sci.*, vol. 51, no. 12, pp. 6715–6721, 2010.

[4] H. Liu, Y. Xu, D. W. K. Wong, and J. Liu, "Effective drusen segmentation from fundus images for age-related macular degeneration screening," in *Proc. Asian Conf. Comput. Vis.*, 2014, pp. 483–498.

[5] Z. B. Sbeh, L. D. Cohen, G. Mimoun, and G. Coscas, "A new approach of geodesic reconstruction for drusen segmentation in eye fundus images," *IEEE Trans. Med. Imag.*, vol. 20, no. 12, pp. 1321–1333, Dec. 2001.

[6] R. T. Smith *et al.*, "Automated detection of macular drusen using geometric background leveling and threshold selection," *Arch. Ophthalmol.*, vol. 123, no. 2, pp. 200–206, 2005.

[7] N. Dey, M. Pal, and A. K. Das, "A session based blind watermarking technique within the NROI of retinal fundus images for authentication using DWT, spread spectrum and harris corner detection," *Comput. Sci.*, vol. 2, pp. 749–757, Sep. 2012.

[8] S. H. Sarks, J. J. Arnold, M. C. Killingsworth, and J. P. Sarks, "Early drusen formation in the normal and aging eye and their relation to age related maculopathy: A clinicopathological study," *Brit. J. Ophthalmol.*, vol. 83, no. 3, pp. 358–368, 1999.

[9] H. Al-Hussaini, M. Schneiders, P. Lundh, and G. Jeffery, "Drusen are associated with local and distant disruptions to human retinal pigment epithelium cells," *Experim. Eye Res.*, vol. 88, no. 3, pp. 610–612, 2009.

[10] H. E. Grossniklaus *et al.*, "Immunohistochemical and histochemical properties of surgically excised subretinal neovascular membranes in age-related macular degeneration," *Amer. J. Ophthalmol.*, vol. 114, no. 4, pp. 464–472, 1992.

[11] N. Jain *et al.*, "Quantitative comparison of drusen segmented on SD-OCT versus drusen delineated on color fundus photographs," *Invest. Ophthalmol. Vis. Sci.*, vol. 51, no. 10, pp. 4875–4883, 2010.

[12] Ujjwal, K. S. Deepak, A. Chakravarty, and J. Sivaswamy, "Visual saliency based bright lesion detection and discrimination in retinal images," in *Proc. IEEE Int. Symp. Biomed. Imag.*, Apr. 2013, pp. 1436–1439.

[13] E. S. Barriga *et al.*, "Multi-scale AM-FM for lesion phenotyping on age-related macular degeneration," in *Proc. IEEE Int. Symp. Comput.-Based Med. Syst.*, 2009, pp. 1–5.

[14] K. Rapantzikos, M. Zervakis, and K. Balas, "Detection and segmentation of drusen deposits on human retina: Potential in the diagnosis of age-related macular degeneration," *Med. Image Anal.*, vol. 7, no. 1, pp. 95–108, 2003.

[15] D. S. Shin, N. B. Javornik, and J. W. Berger, "Computer-assisted, interactive fundus image processing for macular drusen quantitation," *Ophthalmology*, vol. 106, no. 6, pp. 1119–1125, 1999.

[16] R. T. Smith, T. Nagasaki, J. R. Sparrow, I. Barbazetto, C. C. Klaver, and J. K. Chan, "A method of drusen measurement based on the geometry of fundus reflectance," *Biomed. Eng. Online*, vol. 2, no. 1, p. 10, 2003.

[17] A. Thdibaoui, A. Rajn, and P. Bunel, "A fuzzy logic approach to drusen detection in retinal angiographic images," in *Proc. Int. Conf. Pattern Recognit.*, 2000, pp. 748–751.

[18] K. Sharma and J. Virmani, *A Decision Support System for Classification Normal Med. Renal Disease Using Ultrasound Images: A Decision Support System for Med. Renal Diseases*. Hershey, PA, USA: IGI Global, 2017.

[19] S. Hemalatha and S. M. Anouncia, "Unsupervised segmentation of remote sensing images using FD based texture analysis model and ISODATA," *Int. J. Ambient Comput. Intell.*, vol. 8, no. 3, pp. 58–75, 2017.

[20] J. Lian *et al.*, "Measuring spectral inconsistency of multispectral images for detection and segmentation of retinal degenerative changes," *Sci. Rep.*, vol. 7, no. 1, p. 11288, 2017.

[21] X. Dong, H. Zhang, J. Sun, and W. Wan, "A two-stage learning approach to face recognition," *J. Vis. Commun. Image Represent.*, vol. 43, pp. 21–29, Feb. 2017.

[22] D. E. Freund, N. Bressler, and P. Burlina, "Automated detection of drusen in the macula," in *Proc. IEEE Int. Conf. Symp. Biomed. Imag., From Nano Macro*, Jul. 2009, pp. 61–64.

[23] J. Cheng *et al.*, "Early age-related macular degeneration detection by focal biologically inspired feature," in *Proc. IEEE Int. Conf. Image Process.*, Oct. 2012, pp. 2805–2808.

[24] Y. Zheng *et al.*, "An automated drusen detection system for classifying age-related macular degeneration with color fundus photographs," in *Proc. IEEE 10th Int. Symp. Biomed. Imag. (ISBI)*, Apr. 2013, pp. 1448–1451.

[25] Y. Zheng, H. Wang, J. Wu, J. Gao, and J. C. Gee, "Multiscale analysis revisited: Detection of drusen and vessel in digital retinal images," in *Proc. IEEE Int. Symp. on Biomed. Imag., From Nano to Macro*, Apr. 2011, pp. 689–692.

[26] K. Simonyan, A. Vedaldi, and A. Zisserman, "Learning local feature descriptors using convex optimisation," *IEEE Trans. Pattern Anal. Mach. Intell.*, vol. 36, no. 8, pp. 1573–1585, Aug. 2014.

[27] Z. Lei, M. Pietikäinen, and S. Z. Li, "Learning discriminant face descriptor," *IEEE Trans. Pattern Anal. Mach. Intell.*, vol. 36, no. 3, pp. 289–302, Feb. 2014.

[28] P. Wang, J. Wang, G. Zeng, and W. Xu, "Supervised kernel descriptors for visual recognition," in *Proc. IEEE Conf. Comput. Vis. Pattern Recognit.*, Jun. 2013, pp. 2858–2865.

[29] H. Zhang and J. Lu, "Semi-supervised fuzzy clustering: A kernel-based approach," *Knowl.-Based Syst.*, vol. 22, no. 6, pp. 477–481, 2009.
[30] Q. Mei, H. Zhang, and C. Liang, "A discriminative feature extraction approach for tumor classification using gene expression data," *Current Bioinf.*, vol. 11, no. 5, pp. 561–570, 2016.
[31] X. Zhen, M. Yu, A. Islam, M. Bhaduri, I. Chan, and S. Li, "Descriptor learning via supervised manifold regularization for multioutput regression," *IEEE Trans. Neural Netw. Learn. Syst.*, vol. 28, no. 9, pp. 2035–2047, Sep. 2017.
[32] J. Ye, "Generalized low rank approximations of matrices," *Mach. Learn.*, vol. 61, nos. 1–3, pp. 167–191, 2005.
[33] M. W. Berry, S. T. Dumais, and G. W. O'Brien, "Using linear algebra for intelligent information retrieval," *Soc. Ind. Appl. Math.*, vol. 37, no. 4, pp. 573–595, 1995.
[34] Z. Zhang and K. Zhao, "Low-rank matrix approximation with manifold regularization," *IEEE Trans. Pattern Anal. Mach. Intell.*, vol. 35, no. 7, pp. 1717–1729, Jul. 2013.
[35] Y. Wang, H. Zhang, and F. Yang, "A weighted sparse neighbourhood-preserving projections for face recognition," *IETE J. Res.*, vol. 63, no. 3, pp. 1–10, 2017.
[36] M. Belkin and P. Niyogi, "Laplacian eigenmaps and spectral techniques for embedding and clustering," in *Proc. Adv. Neural Inf. Process. Syst.*, 2002, pp. 585–591.
[37] *Stare-Structured Analysis of the Retina*. Accessed: Jan. 2017. [Online]. Available: http://cecas.clemson.edu/~ahoover/stare/
[38] M. M. Fraz *et al.*, "Blood vessel segmentation methodologies in retinal images–a survey," *Comput. Methods Programs Biomed.*, vol. 108, no. 1, pp. 407–433, 2012.
[39] S. Lu and J. H. Lim, "Automatic optic disc detection from retinal images by a line operator," *IEEE Trans. Bio-Med. Eng.*, vol. 58, no. 1, pp. 88–94, Jan. 2011.
[40] U. M. Akram and S. A. Khan, "Automated detection of dark and bright lesions in retinal images for early detection of diabetic retinopathy," *J. Med. Syst.*, vol. 36, no. 5, pp. 3151–3162, 2012.
[41] X. Zhu, R. M. Rangayyan, and A. L. Ells, "Digital image processing for ophthalmology: Detection of the optic nerve head," *Synth. Lectures Biomed. Eng.*, vol. 6, no. 1, pp. 1–106, 2011.
[42] *Drive: Digital Retinal Images for Vessel Extraction*. Accessed: Oct. 2017. [Online]. Available: https://www.isi.uu.nl/Research/Databases/DRIVE/
[43] J. Staal, M. D. Abramoff, M. Niemeijer, M. A. Viergever, and B. van Ginneken, "Ridge-based vessel segmentation in color images of the retina," *IEEE Trans. Med. Imag.*, vol. 23, no. 4, pp. 501–509, Apr. 2004.
[44] A. H. Briggs, "Handling uncertainty in cost-effectiveness models," *Pharmacoeconomics*, vol. 17, no. 5, pp. 479–500, 2000.
[45] N. Dey, A. B. Roy, M. Pal, and A. Das, "Fcm based blood vessel segmentation method for retinal images," *Int. J. Comput. Sci. Netw.*, vol. 1, no. 3, Sep. 2012.
[46] Y. He, Y. Zheng, Y. Zhao, Y. Ren, J. Lian, and J. Gee, "Retinal image denoising via bilateral filter with a spatial kernel of optimally oriented line spread function," *Comput. Math. Methods Med.*, to be published.
[47] H. Liu, Y. Xu, D. W. K. Wong, and J. Liu, "Growcut-based drusen segmentation for age-related macular degeneration detection," in *Proc. Vis. Commun. Image Process. Conf.*, 2015, pp. 161–164.
[48] A. D. Mora, P. M. Vieira, A. Manivannan, and J. M. Fonseca, "Automated drusen detection in retinal images using analytical modelling algorithms," *Biomed. Eng. Online*, vol. 10, no. 1, p. 59, 2011.
[49] K. Kumari and D. Mittal, "Drusen quantification for early identification of age related macular degeneration," *Adv. Image Video Process.*, vol. 3, no. 3, p. 28, 2015.
[50] A. Bhuiyan *et al.*, "Drusen detection and quantification for early identification of age related macular degeneration using color fundus imaging," *Clin. Experim. Ophthalmol.*, vol. 4, no. 305, p. 2, 2013.
[51] H. Wang, S. Yan, D. Xu, X. Tang, and T. Huang, "Trace ratio vs. ratio trace for dimensionality reduction," in *Proc. IEEE Conf. Comput. Vis. Pattern Recognit. (CVPR)*, Jun. 2007, pp. 1–8.
[52] A. Edelman, T. A. Arias, and S. T. Smith, "The geometry of algorithms with orthogonality constraints," *SIAM J. Matrix Anal. Appl.*, vol. 20, no. 2, pp. 303–353, 1998.

XIUXIU REN is currently pursuing the master's degree with the School of Information Science and Engineering, Shandong Normal University, China. Her current research interests include image processing.

YUANJIE ZHENG is currently a Professor with the School of Information Science and Engineering, Shandong Normal University and a Taishan Scholar of People's Government of Shandong Province of China. He was a Senior Research Investigator with the Perelman School of Medicine, University of Pennsylvania. He is also serving as a Vice Dean of the School of Information Science and Technology and the Institute of Life Sciences, Shandong Normal University. His research interests include medical image analysis, translational medicine, computer vision, and computational photography. His ultimate research goal is to enhance patient care by creating algorithms for automatically quantifying and generalizing the information latent in various medical images for tasks, such as disease analysis and surgical planning through the applications of computer vision and machine learning approaches to medical image analysis tasks and development of strategies for image-guided intervention/surgery.

YANNA ZHAO received the Ph.D. degree in signal and information processing from Shandong University in 2015. She was a Visiting Scholar with the Institute of Image Processing and Pattern Recognition, Shanghai Jiao Tong University, from 2011 to 2015. She is currently a Lecturer with the School of Information Science and Engineering, Shandong Normal University. Her current research interests include computer vision, pattern recognition, and image processing.

CHAO LUO received the master's degree in computer science from the Dalian University of Technology, China, in 2005, and the Ph.D. degree from the Faculty of Electronic Information and Electrical Engineering, Dalian University of Technology. He is currently an Associate Professor with the School of Information Science and Engineering, Shandong Normal University. His current research interests include systems biology and complex networks.

HONG WANG received the bachelor's and master's degrees in computer software from Tianjin University in 1988, and the Ph.D. degree from the Chinese Academy of Sciences in 2002. She is currently a Professor and a Doctoral Supervisor with the School of Information Science and Engineering, Shandong Normal University. Her current research interests include complex networks, mobile agents, social software, and big data cloud.

JIAN LIAN is currently pursuing the Ph.D. degree with the School of Information Science and Engineering, Shandong Normal University, China. His current research interests include medical image processing.

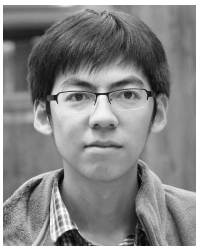

YUNLONG HE is currently pursuing the master's degree with the School of Information Science and Engineering, Shandong Normal University of China. His current research interests include computer vision, medical imaging, and machine learning.